ELSEVIER

International Journal of Mass Spectrometry 177 (1998) 163–174

International Journal of Mass Spectrometry

Relaxation of internally excited high-mass ions simulated under typical quadrupole ion trap storage conditions

Douglas E. Goeringer*, Scott A. McLuckey

Chemical and Analytical Sciences Division, Oak Ridge National Laboratory, Building 5510, MS-6365, Oak Ridge, TN 37831-6365, USA

Received 24 November 1997; accepted 8 May 1998

Abstract

Collisional relaxation of internally excited high-mass (>1 kDa) ions has been simulated under typical quadrupole ion trap storage conditions. Two models have been employed that are expected to bracket the range of cooling rates that prevail for such ions present in ~1 mTorr of room temperature helium. A diffuse scattering model that assumes that the helium target atom thermally equilibrates with the high-mass ion upon collision is expected to yield a maximum cooling rate. A random walk algorithm using the exponential model for inefficient colliders and a relatively small average energy down-step size provides an estimate for the lowest cooling rates that might be expected. The two models give cooling rates that differ by about a factor of three and fall within the range of 200–2000 s^{-1} for the ions and energies considered in the simulations. Unimolecular dissociation rates have also been determined for the same model ions. Random walk simulations employing collisional cooling and dissociation clearly show how a rapid input of internal energy, as with the absorption of an ultraviolet photon, can either result in dissociation of a large fraction of the ions or can lead to an insignificant degree of dissociation, depending largely on the unimolecular dissociation rate of the ion. (Int J Mass Spectrom 177 (1998) 163–174) © 1998 Elsevier Science B.V.

Keywords: Quadrupole ion trap; Helium bath gas; Collisional cooling; Internal relaxation

1. Introduction

The formation and manipulation of high-mass (>1 kDa) ions in mass spectrometry has become commonplace with the increasingly widespread use of electrospray ionization [1–7] and matrix-assisted laser desorption ionization [8–10]. High-mass ions formed by these and other methods are subjected to manipulation and analysis in a variety of instrument types, including, for example, the time-of-flight mass spectrometer [11,12], the Fourier transform ion cyclotron resonance instrument [13], and the radiofrequency quadrupole ion trap (Paul trap) [14]. A number of factors determine the analyzer type most appropriate for a particular measurement [15]. The operational conditions of the various mass analysis tools lead both to the differences in the relative mass analysis performance characteristics between analyzers and to differences in time-frames and propensities for ion-neutral collisions. Among the most commonly used mass analysis tools is the Paul trap. When operated with helium bath gas at roughly 1 mTorr, it stands out as the mass analyzer that yields the largest numbers and rates of ion-neutral collisions.

The intended role of the bath gas in most quadru-

* Corresponding author. E-mail: goeringerde@ornl.gov

PII S1387-3806(98)14043-5

pole ion trap experiments is to reduce ion kinetic energies so that the ion cloud collapses toward the center of the ion trapping volume [16]. This phenomenon improves both resolution and sensitivity for ion populations initially present with large spreads in energy and position. It is particularly important in the capture of ions injected into the ion trapping volume from an external ion source. Various models, all of which assume elastic ion-helium collisions, have been used to describe the translational cooling of ions within the context of ion motion simulations in the quadrupole ion trap [17]. These models are useful for the description of ion motion but, of course, cannot account for important phenomena in the ion trap that result from inelastic ion-helium collisions. Such phenomena include collisional activation of translationally excited ions and the internal relaxation of internally excited ions via the intermolecular vibrational-to-translational energy transfer that takes place between a hot molecule and a thermal helium atom. The former process forms the basis for ion trap collisional activation and likely plays a role in the fragmentation of relatively small and fragile ions upon their injection into an ion trap [18–20]. Fragmentation of ions injected into the ion trap has been interpreted as arising from internal heating of ions via ion-helium collisions during the process of translational cooling [21] along with possible contributions from surface-induced dissociation [22].

Previous work in our laboratory has focused on random walk simulations incorporating inelastic collisions to describe changes in polyatomic ion internal energy distributions associated with ion trap resonance excitation [23] and to model collision-induced dissociation kinetics in the ion trap [24]. In that work, the ion activation and deactivation processes of an initially thermal polyatomic ion population undergoing resonance excitation were studied. In this work, we adapt the random walk algorithm to the removal of excess internal energy from an initially excited high-mass ion. This process has important implications for phenomena that yield internally excited high-mass ions on a transitory basis. That is, in cases in which energy is deposited in relatively rapid fashion (not continuously, as in resonance excitation) and the ions are subsequently stored in the presence of the bath gas. Examples of such phenomena include pulsed laser excitation, ion injection into the ion trap, and ion–ion reactions. Although fragmentation upon injection of ions into the ion trap has been observed for relatively small polyatomic ions, we have not observed this phenomenon with high-mass ions derived from electrospray, even for relatively fragile noncovalently bound complexes [25,26]. Furthermore, we have recently reported a number of studies involving multiply charged bio-ions that undergo multiple highly exothermic ion–ion reactions without detectable fragmentation [27]. These ions have included noncovalently bound complexes [28]. On the other hand, we have observed extensive fragmentation of oligonucleotide anions that transfer electrons to cations such as ionized rare gases [29]. The extent of fragmentation appears to be a function of reaction exothermicity and bio-ion size [30,31]. Internal cooling of initially excited ions via collisions with helium must also play a role.

Intermolecular energy transfer from vibrationally excited species (both neutral and charged molecules) to cold bath gas molecules has been the subject of theoretical and experimental studies for some time [32–35], but collisional vibrational energy transfer for large biopolymer ions has become of interest only relatively recently. Of particular note is the work of Marzluff et al. [36] who modeled the translation-to-vibration process for collisional activation of peptide ions and showed energy transfer efficiencies $>50\%$. Furthermore, energy transfer tended to increase with the size of the ion. The rate of the vibration-to-translation process, which is of interest in this work, is also dependent on the degree of collision inelasticity. Whether fragmentation of an ion is observed after a transitory input of energy is determined both by the unimolecular dissociation rate and the relaxation rate, which is usually dominated by the ion-helium collision process in the ion trap. Although the applicability to high-mass ions of the energy randomization hypothesis in statistical theories of unimolecular decomposition remains an open question [37], calculations based on such theories predict the reduction of unimolecular dissociation rates with ion size [38]. Fur-

thermore, increasing collision cross section with ion size tends to lead to an increase in the collision rate in the Paul trap. Thus, the minimal fragmentation of high-mass bio-ions alluded to above has been attributed to their relatively rapid rate of internal energy relaxation compared with unimolecular dissociation [28,31,39]. In this article, both a random walk algorithm employing the exponential model for inefficient colliders and a simple statistical model are used to obtain quantitative predictions of the collisional relaxation rates for high-mass ions. Results reveal that polypeptide ions less than ~4000 Da can cool from 450 to 300 K (ion internal temperature) in <10 ms at 1 mTorr He pressure, and the unimolecular dissociation rate constants fall by orders of magnitude over the corresponding internal energy range.

2. Collisional cooling models and RRKM parameters

2.1. Vibrational energy transfer kinetics

For the purpose of this study, it is assumed that the internal energy present in ions (AB^+) is distributed statistically among the various vibrational modes and that energy can move freely about within statistical phase-space (i.e. the energy randomization hypothesis of Rice, Ramsberger, Kassel, Marhus (RRKM) theory [40]). The excited ions (AB^+*), which are arbitrarily given a charge of +1 for this arguement, can undergo unimolecular dissociation to form fragment ions (A^+) and neutral particles (B) and/or de-excitation via radiative relaxation and intermolecular vibrational energy transfer during collisions with neutral species (M). The general kinetic scheme for such processes is

$$AB^+* + M \underset{k_{act}}{\overset{k_{rel}}{\rightleftarrows}} AB^+ + M$$

$$AB^+* \xrightarrow{k_{rad}} AB^+$$

$$AB^+* \xrightarrow{k_{uni}} A^+ + B$$

where $k_{act}[M]$ is the collisional activation rate, $k_{rel}[M]$ is the collisional deactivation rate, k_{rad} is the radiative relaxation rate constant, and k_{uni} is the unimolecular dissociation rate constant. The differential equation for change in $[AB^+*]$ is given by Eq. (1).

$$\frac{(d[AB^+*]/[AB^+*])}{dt} = k_{act}[M]\frac{[AB^+]}{[AB^+*]} - (k_{rel}[M] + k_{rad} + k_{uni}) \quad (1)$$

An apparent (pseudo-first order) rate constant k_{app} for the overall relaxation of vibrationally excited ions can then be defined by Eq. (2),

$$k_{app} = k_{rel}[M] + k_{rad} \quad (2)$$

and a plot of k_{app} versus $[M]$ should be linear with a slope equal to the (phenomenologic) bimolecular collisional cooling rate constant k_{rel} and an intercept equal to k_{rad}.

Most of the internal energy in polyatomic molecules occupies infrared inactive modes, with the radiative intensity from active modes scaling linearly with the total number of oscillators. Dunbar [41] has examined methods for calculating the rate of infrared radiative cooling of hot polyatomic ions based on a weakly coupled harmonic oscillator model. The energy radiated per second $W_i^{v,v-1}$ during the transition from vibrational level v to $v - 1$ of oscillator mode i can be expressed by

$$W_i^{v,v-1} = h \cdot c \cdot \overline{\nu_i} \cdot P_i^v \cdot A^{v,v-1}$$

where h is Planck's constant, c is the speed of light, $\overline{\nu_i}$ is the photon frequency expressed in cm^{-1}, and P_i^v is the statistical probability of finding mode i in quantum state v. Summing $W_i^{v,v-1}$ over all occupied levels of all modes then gives the total energy emission rate. The Einstein coefficient for spontaneous emission $A^{v,v-1}$ is related to the experimentally determined infrared band intensity A_i; however, integrated intensity data are not available for the model ions used in this study, that is, multiple alanine-glycine (AG) dipeptide units. Thus, we used Dunbar's standard hydrocarbon model [42] to estimate the infrared

active transition frequencies and A_i values for $(AG)_n$. Radiative relaxation curves were then calculated for $(AG)_n$ ions (n = 8, 16, 24, 32). Results indicated that for such ions, vibrational relaxation via infrared radiative cooling occurs on a time scale over two orders of magnitude longer than relaxation because of collisional processes at 1 mTorr helium bath gas pressure (see below). Thus, k_{rad} is assumed to be insignificant compared with collisional processes and k_{app} can be expressed to a good approximation by Eq. (3).

$$k_{app} = k_{rel}\,[M] \tag{3}$$

Note that k_{app} reflects the average relaxation rate for an ensemble of ions. However, vibrational relaxation actually proceeds via a discrete state-to-state process that occurs in a stepwise manner. The kinetics for such a process can be written as a coupled set of differential equations [Eq. (4)] for the change in individual energy levels $[AB^+]_j$,

$$\frac{(d[AB^+]_j/[AB^+]_j)}{dt} = \sum_{i\neq j} R_{ij}\frac{[AB^+]_i}{[AB^+]_j} - \left(\sum_{i\neq j} R_{ji} + k_{uni_j}\right) \tag{4}$$

where R_{ij} is the microscopic rate of collisional energy transfer from energy level E_i to E_j, and k_{uni_j} is energy-dependent and zero below the critical energy. R_{ij} can be further defined in terms of a collisional energy transfer probability function P_{ij} (for energy up- or down-steps) and ion-neutral collision frequency v as given by Eq. (5).

$$R_{ij} = vP_{ij} \tag{5}$$

Combining Eqs. (4) and (5) and summing over all energy levels gives Eq. (6) describing the overall rate,

$$\frac{\Sigma_j\,(d[AB^+]_j/[AB^+]_j)}{dt} = v\times\sum_j\sum_{i\neq j} P_{ij}\frac{[AB^+]_i}{[AB^+]_j} - \sum_j\left(v\sum_{i\neq j} P_{ji} + k_{uni_j}\right) \tag{6}$$

and k_{app} for vibrational relaxation via collisional cooling is given by Eq. (7).

$$k_{app} = v\sum_j\sum_{i\neq j} P_{ji} \tag{7}$$

Comparing Eqs. (3) and (7) gives Eq. (8),

$$k_{rel}\,[M] = v\sum_j\sum_{i\neq j} P_{ji} \tag{8}$$

indicating that the bimolecular collisional cooling rate $k_{rel}[M]$ is equal to the sum of the rates of collisional energy transfer from all energy levels. The total internal energy

$$E\propto\sum_j [AB^+]_j$$

so the overall rate of change in internal energy $(dE/E)/dt$ is given by Eq. (9).

$$\frac{dE/E}{dt} = v\sum_j\sum_{i\neq j} P_{ij}\times\frac{[AB^+]_i}{[AB^+]_j} - \sum_j\left(v\sum_{i\neq j} P_{ji} + k_{uni_j}\right) \tag{9}$$

Thus, simulation of the state-to-state energy transfer steps produced by collisional processes enables k_{app} to be obtained by following the resulting internal energy evolution and determining the slope of $a - \ln(E_t/E_0)$ versus t plot. The random walk procedure described below is just such a simulation for collisional relaxation.

2.2. Random walk model

The set of kinetic equations (6) can be solved using the exact stochastic method (ESM) of Gillespie to simulate a random walk in vibrational energy space [43]. The fractional energy lost from a highly excited polyatomic ion upon collision with a monatomic gas is expected to be small, so for the random walk simulation we chose to use the exponential model for inefficient colliders [44] in which P_{ij} decreases exponentially with energy step size. A simple exponential model like this may not, in fact, best describe the

situation. For example, a displaced Gaussian functional form has been shown to be in better accord with data involving relatively small polyatomic ions [45,46]. However, in any case, the k_{app} derived from the random walk model is expected to be much more sensitive to the mean value of the step size than to the functional form of P_{ij} [47].

The exponential model for inefficient colliders employs an expression for P_{ij} for energy down-steps given by Eq. (10),

$$P_{ij} = \frac{\exp[-(E_i - E_j)/\alpha]}{C_i}, \quad E_j < E_i \tag{10}$$

where C_i is an energy-dependent normalization factor (see below). For P_{ij} of the form given by Eq. (10), the collisional relaxation rate is largely determined by the size of α, which is seen to be equal to the average energy lost on a down-step, $\langle \Delta E_d \rangle$.

$$\langle \Delta E_d \rangle \equiv \frac{\int_{E_i}^{0} (E_i - E)\exp(-(E_i - E)/\alpha)\ dE}{\int_{E_i}^{0} \exp(-(E_i - E)/\alpha)\ dE} = \alpha \tag{11}$$

At equilibrium, microscopic reversibility gives

$$\nu P_{ij} B_i = \nu P_{ji} B_j,$$

$$B_g = \frac{\rho_g \exp[-E_g/(kT_{int})]}{Q_{vib}},\ g = i,j \tag{12}$$

where k is the Boltzmann constant, ρ_g is the density of states at energy E_g, and Q_{vib} is the vibrational partition function at ion *internal* temperature T_{int}. Combining Eqs. (10) and (12) gives Eq. (13),

$$P_{ij} = \frac{\exp(-[E_j - E_i]/\alpha) \times \rho_j \exp[-E_j/(k \times T_{int})]}{\rho_i \times C_j \exp[-E_i/(k \times T_{int})]},$$

$$E_j > E_i \tag{13}$$

Furthermore, normalization requires that

$$\int_0^\infty P_{ij}\ dE = \int_E^0 P_{ij}\ dE + \int_E^\infty P_{ij}\ dE = 1 \tag{14}$$

$$E_j < E_i \qquad E_j > E_i$$

so that the specific form for C_i can be obtained by combining Eqs. (10), (13), and (14) to give the integral Eq. (15),

$$C_i = \int_{E_i}^{0} \exp\left(\frac{-[E_i - E]}{\alpha}\right) dE + \int_{E_i}^{\infty} \frac{C_i\, \rho_j \exp(-[E - E_i]\,[(\alpha + k\ T_{int})/(\alpha\ k\ T_{int})])}{C_j\, \rho_i}\, dE \tag{15}$$

which can be solved using the finite difference method of Gilbert and King [48]. Finally, curves can be contructed for the energy down-step P_d and up-step P_u probabilities:

$$P_{d_i} = \frac{\int_{E_i}^{0} \exp(-[E_i - E]/\alpha)\ dE}{C_i} \tag{16}$$

$$P_{u_i} = \frac{\int_{E_i}^{\infty} \frac{C_i\, \rho_j \exp(-[E - E_i]\,[(\alpha + k\ T_{int})/(\alpha\ k\ T_{int})])}{C_j\, \rho_i}\, dE}{C_i} \tag{17}$$

The expression for α used in this work assumes a linear dependence on the internal temperature above thermal of the form,

$$\alpha = \frac{3}{4} k\ T_M + \frac{5}{8} k\ (T_{int} - T_M) \tag{18}$$

where T_M is the neutral collision gas temperature. A minimum criterion for the expression for α is that the random walk simulations resulting from its use match the corresponding distributions calculated from the Boltzmann equation over the range of interest for T_{int}.

Eq. (18) meets this criterion. Because of the dearth of experimental data for collisional relaxation of large polymeric ions, we chose not to attempt to derive more sophisticated expressions for α based on, for example, restricted statistical theories of vibrational energy transfer [49–51] that take into account physical and chemical properties of the target, such as mass, polarizability, number of degrees of freedom, and so forth. Rather, in the absence of data to guide the development of such an expression, we chose to use a physically realistic expression that shows a finite average energy down-step size when $T_{\text{int}} = T_M$ and that increases as the difference between T_{int} and T_M increases. Furthermore, the constants in the expression were selected to yield an average energy down-step size that falls at the low end ($\sim$100 cm^{-1}) of the range of values reported for relatively small polyatomic ions in collisions with helium ($\sim$100–350 cm^{-1}) [47,52]. In so doing, we expect that the random walk model using Eq. (18) tends to underestimate k_{app} because the use of a relatively small down-step size simulates collisions of low inelasticity. The simple diffuse collision model described below, on the other hand, simulates highly inelastic collisions and is expected to yield the highest realistic collisional cooling rates. The two models are therefore expected to bracket the range of collisional cooling rates under common Paul trap operating conditions.

In the ESM, the random time interval between ion-neutral collisions τ is

$$\tau = \frac{1}{\nu} ln\left(\frac{1}{r_1}\right) \tag{19}$$

where r_1 is a random number from the unit-interval distribution (equal probability for any number between 0 and 1). From ion mobility theory,

$$\nu = \frac{4}{3} n_M \times \sqrt{\frac{8\ k\ T}{\pi\ \mu}}\ \Omega \tag{20}$$

where n_M is the neutral number density, μ is the ion-neutral reduced mass, and Ω is a collision integral. For rigid-sphere scattering, Ω is equal to the collision cross section σ (projection area). Revercomb and Mason [53] have shown that Ω for rigid-sphere scattering of large ions (i.e. reduced mass, $\mu \approx M$) can be closely approximated by

$$\Omega = \pi\ r_m^2,\ r_m = r_0\left[1 + b_m\left(\frac{m}{M}\right)^{1/3}\right],$$

$$r_0 = 2.1\ \text{Å},\ b_m = 1 \tag{21}$$

More recently, however, Chen et al. [54] have measured bio-ion collision cross sections via energy loss measurements on a triple quadrupole mass spectrometer. Interpreting the results in terms of an aerodynamic drag model, they found that the ion-neutral collisions were described better by diffuse (highly inelastic) rather than specular (rigid-sphere, elastic) scattering [54]. For a given projection area, there is a greater average momentum loss ($\sim$22–25%) per ion-neutral collision via diffuse than specular scattering. Thus, the Ω values calculated with Eq. (21) were multiplied by 0.75 when calculating v values for the simulations. The oligomer molecular weights, numbers of internal degrees of freedom, and collision cross sections used in this work are listed in Table 1.

2.3. Diffuse scattering model

As noted above, Chen et al. [54] have found that ion-neutral collisions of biopolymer ions were described better by diffuse rather than specular scattering. Under diffuse scattering conditions, a helium atom may undergo multiple collisions with the irregular surface of a bio-ion during each ion-neutral interaction event, internal energy loss via V-T energy transfer occurring on each collision. If each helium atom is assumed to approach the ion at $T = T_M$ and to scatter at $T = T_{\text{int}}$, then the total vibrational energy transferred to the neutral during each multiple-collision interaction is $(3/2)k(T_{\text{int}} - T_M)$. Thus, the ion internal energy $E_{n_{\text{col}}}$ after multiple-collision interaction number n_{col} can be calculated from Eq. (22),

$$E_{n_{\text{col}}} = E_{n_{\text{col}}^{-1}} - \frac{3}{2} k(T_{\text{int}} - T_M) \tag{22}$$

where E_0 is the initial internal energy and the interactions are spaced at time intervals determined via Eq.

Table 1
Physical data for $(AG)_n$ ions

Ion	MW (kDa)	Ω (Å^2)[a]	Degrees of freedom
$(AG)_8$	1.043	570	411
$(AG)_{12}$	1.556	720	615
$(AG)_{16}$	2.068	850	819
$(AG)_{20}$	2.581	970	1023
$(AG)_{24}$	3.093	1100	1227
$(AG)_{28}$	3.606	1200	1431
$(AG)_{32}$	4.118	1300	1635

[a] $0.75 \times \Omega_{\text{Eq. (19)}}$.

(19). The diffuse scattering model assumes that the bath gas thermally equilibrates with the polyatomic ion. This picture represents the maximum realistic degree of collision inelasticity and constitutes a reasonable order of magnitude model given the high collision inelasticity suggested by Marzluff et al. [36] for collisional activation of high mass ions.

2.4. RRKM calculations

The group of model biopolymer ions used in this study consisted of multiple alanine-glycine (AG) dipeptide units as described by Griffin and McAdoo [38]. Thus, the model for the $(AG)_n$ polypeptide ion consisted of the 54 AG frequencies and $n - 1$ degenerate sets of glycyl-alanyl (GA) frequencies. Cleavage of the C-terminal peptide bond was used as the reaction coordinate. Transition state frequencies were adjusted by modifying AG frequencies associated with the dissociating (first A–G) peptide bond, specifying the CN stretch as the reaction coordinate, and adding the $n - 1$ GA frequencies. Unimolecular dissociation rate constants were determined via RRKM calculations in which the steepest descent method was used to make density of states estimates [55,56].

3. Results and discussion

With the necessary parameters in hand, the internal energy evolution for an individual $(AG)_n$ ion was monitored over a series of random time intervals [Eq. (19)] corresponding to the periods between ion-neutral collisions. Subsequent to each collision, Barker's Monte Carlo technique [57] was used to randomize the energy-step direction and magnitude within the constraints imposed by Eqs. (16) and (17). More specifically, for each ion-neutral collision if a second random number r_2 (from the unit interval distribution) was less than P_{d_i} [Eq. (16)], an energy down-step was selected. Furthermore, Eq. (23)

$$r_3 = \frac{\int_0^{\Delta E_{d_i}} \exp(-\Delta E/\alpha_i)\, d(\Delta E)}{\int_0^{E_i} \exp(-\Delta E/\alpha_i)\, d(\Delta E)} \tag{23}$$

where r_3 is another random number from the unit interval distribution, was solved analytically [Eq. (24)]

$$\Delta E_{d_i} = -\alpha_i \ln\left\{1 - r_3\left[1 - \exp\left(\frac{-E_i}{\alpha_i}\right)\right]\right\} \tag{24}$$

and used to determine the magnitude ΔE_d of that down-step. For cases in which an energy up-step was selected (i.e. $r_2 > P_{d_i}$), expressions similar to Eqs. (23) and (24) [57] were also used to determine the up-step magnitude. Thus, the overall trend for any random walk was a decline in internal energy via energy-steps described by an exponential probability distribution having an average down-step size α, despite the fact that any individual collision might actually result in an energy down- or up-step somewhat different than α. Note, however, that a steady-state condition in which up-steps were balanced by down-steps was ultimately reached at thermal energy because $P_{u_i} = 0.5$ at $T_{\text{int}} = T_M$. Thus, the ion executed a random walk in internal energy-space similar to the events believed to occur in the actual physical process. The results from a series (250) of such random walks, each with the same initial conditions, were averaged to obtain a smooth decay curve.

Fig. 1(a) shows a typical example of the internal energy versus time plot from a (single) simulation of the internal energy relaxation for $(AG)_{16}$ because of multiple collisions with helium atoms at 10^{-3} Torr ($\nu = 4.6 \times 10^5$ s^{-1}) and 300 K (identical bath gas conditions were used in all simulations reported here). The ion had an initial internal energy of 7.2 eV, which

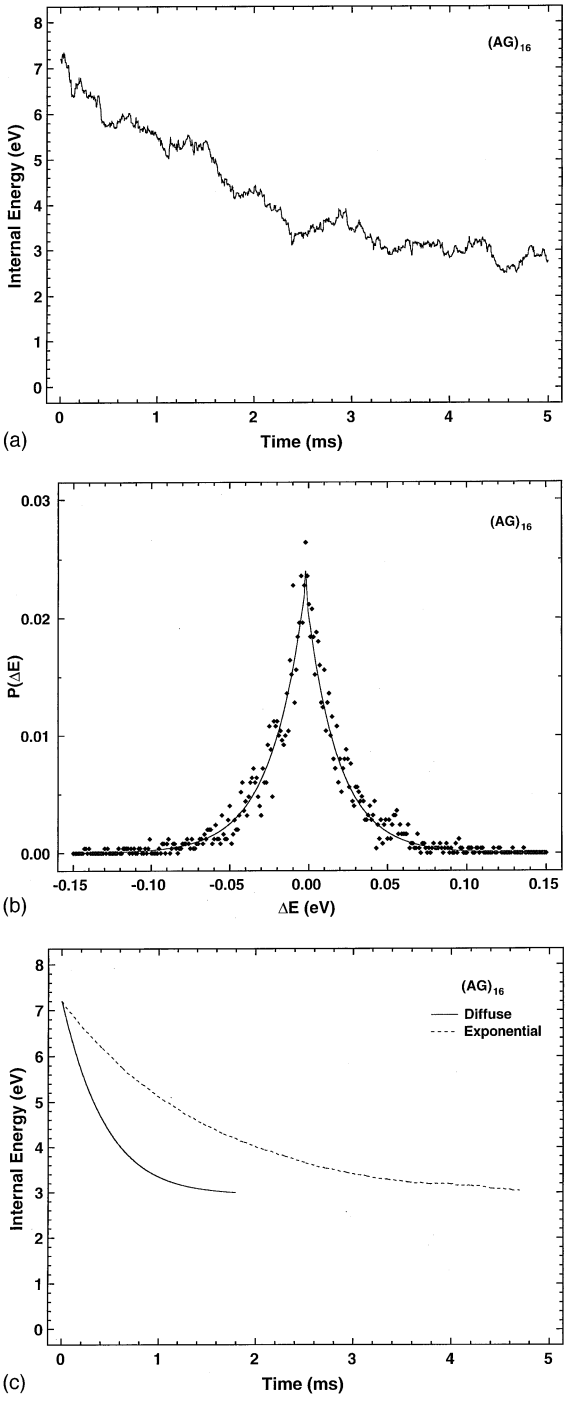

Fig. 1. (a) Random walk simulation of internal energy cooling, via collisions with thermal (300 K) He atoms (10^{-3} Torr), for an $(AG)_{16}$ ion having an initial internal energy equal to the average for a Boltzmann distribution at 450 K. The exponential model for inefficient colliders was used for the vibrational–translational energy transfer process. (b) Results from (a) histogrammed to give the probability $P(\Delta E)$ of an energy transition as a function of energy-step size ΔE. Note that the probability reaches a maximum for an elastic collision (i.e. $\Delta E = 0$ eV). (c) Comparison of internal energy cooling curves for $(AG)_{16}$ obtained using the exponential model for inefficient colliders and the diffuse scattering model. The two models are expected to bracket the range of cooling rates observed under common Paul trap operating conditions.

corresponds to an internal temperature of 450 K. A histogram of the corresponding energy-step sizes is shown in Fig. 1(b); its exponential character results from use of the exponential model for inefficient colliders with an α value given by Eq. (18). Fig. 1(c) compares the smooth internal energy relaxation curve for $(AG)_{16}$ obtained by averaging 250 random walk simulations with the corresponding curve calculated using the diffuse collision model for collisional energy transfer.

Collisional relaxation curves for $(AG)_n$ [$n = 8$ ($\sim$1 kDa), $n = 16$ ($\sim$2 kDa), $n = 24$ ($\sim$3 kDa), and $n = 32$ ($\sim$4 kDa)] ions having the same initial internal temperature (450 K) are compared in Fig. 2. The relaxation time increases with size despite the same trend in the ion-neutral collision frequency because the difference in the initial and thermal internal energies increases with size more rapidly. The relaxation curves in Fig. 2 can be used to obtain apparent cooling rates by plotting $-\ln(E_{\mathrm{int}_t}/E_{\mathrm{int}_0})$ as a function of relaxation time; the slope of the resulting line corresponds to k_{app} ($= k_{\mathrm{rel}}[M]$). Apparent cooling rate constants for $(AG)_8$, $(AG)_{12}$, $(AG)_{16}$, $(AG)_{20}$, $(AG)_{24}$, $(AG)_{28}$, and $(AG)_{32}$ obtained from such plots over the T_{int} range 450–350 K are listed in Table 2 along with the corresponding ion-neutral collision frequencies. Quenching efficiencies ϕ can be obtained from these results via the expression $\phi = k_{\mathrm{app}}/v$. Table 2 lists k_{app} values obtained from both the random walk simulation and the diffuse scattering model for two scenarios. In one case, all parent ions begin with energies corresponding to the average energy at 450 K. In the other scenario, parent ions begin with energies corresponding to the average internal energy of an ion at 300 K plus 4 eV. The latter scenario is intended to simulate an experiment in which a thermalized ion absorbs a 308 nm photon.

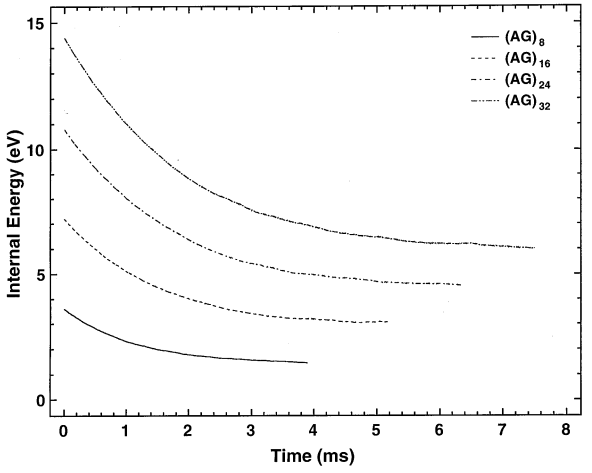

Fig. 2. Composite cooling curves for 450 K $(AG)_n$ ions (n = 8, 16, 24, 32) in 10^{-3} Torr He at 300 K. Each curve is the average of 250 random walk simulations similar to the single curve in Fig. 1(a).

Both models give cooling rates of the same order of magnitude and, as expected, the random walk model gives lower apparent cooling rates (by about a factor of three) than the diffuse collision model.

The extent to which fragmentation competes with cooling is determined by the relative magnitudes of the cooling rate and the unimolecular dissociation rates over the relevant internal energy range. RRKM theory was used to calculate the unimolecular dissociation rate constants k_{uni} for the $(AG)_8$, $(AG)_{12}$, $(AG)_{16}$, $(AG)_{20}$, $(AG)_{24}$, $(AG)_{28}$, and $(AG)_{32}$ ions; the critical energy was fixed at 1 eV. RRKM calculations were performed for each oligomer using the average internal energy at 450 K and again using an internal energy equal to the average internal energy at 300 K plus 4 eV. The values are listed in Table 3. At a given internal energy, RRKM theory predicts that large ions fragment much more slowly than small ions. At a given temperature, however, dissociation rates are far less sensitive to ion size than are rates at constant energy because the increase in internal energy with size for a given temperature compensates for the increase in the density of states. An important scenario in many experimental situations is intermediate between the two extremes of ions with constant internal energy and ions with a constant internal temperature, namely, the situation in which ions at the bath gas temperature are subjected to a rapid input of internal energy. Such a scenario is exemplified well by a UV photodissociation experiment while other

Table 3
Unimolecular dissociation rate constants for $(AG)_n$ ions calculated from RRKM theory

Ion	k_{uni} (s^{-1}) (450 K)	k_{uni} (s^{-1}) (300 K + 4 eV)
$(AG)_8$	9.3	3,700
$(AG)_{12}$	19	150
$(AG)_{16}$	26	16
$(AG)_{20}$	32	3.4
$(AG)_{24}$	36	1.0
$(AG)_{28}$	39	0.40
$(AG)_{32}$	42	0.18

Table 2
Rate constants for collisional cooling of $(AG)_n$ ions determined via random walk simulation and ion-helium collision frequencies at 1 mTorr

Ion	k_{app}[a,b] (450 K)	k_{app}[a,c] (450 K)	k_{app}[a,b] (300 K + 4 eV)	k_{app}[a,c] (300 K + 4 eV)	ν[a]
$(AG)_8$	530	1700	610	2000	3.1×10^5
$(AG)_{12}$	430	1400	470	1500	3.9×10^5
$(AG)_{16}$	390	1300	380	1300	4.6×10^5
$(AG)_{20}$	360	1200	310	1100	5.2×10^5
$(AG)_{24}$	330	1100	270	910	5.8×10^5
$(AG)_{28}$	310	1000	240	800	6.4×10^5
$(AG)_{32}$	290	960	210	710	6.9×10^5

Quenching efficiency, $\phi = k_{app}/\nu$.
[a] s^{-1}.
[b] Exponential model.
[c] Diffuse model.

phenomena, such as a highly exothermic ion-ion reaction, share similarities. The calculation of k_{uni} using the average internal energy at 300 K plus 4 eV is intended to simulate this type of scenario.

Although the k_{uni}(450 K) values are significantly smaller than the k_{app} values predicted from either the random walk simulation or the diffuse collision model for all oligomer sizes, the k_{uni}(300 K + 4 eV) value for the $(AG)_8$ exceeds the k_{app} values from both models. As oligomer size increases the k_{uni}(300 K + 4 eV) values decrease dramatically reflecting the high sensitivity of k_{uni}(300 K + 4 eV) to the number of degrees of freedom in the ion. Fig. 4 shows a plot of dissociation rates, k_{uni}(300 K + 4 eV), and collisional cooling rates, k_{app}(300 K + 4 eV), as a function of n for the various $(AG)_n$-mers. It is clear from this plot that although the k_{app} values decrease with increasing n, the k_{uni} values decrease much more rapidly. The plot clearly suggests that ions must be activated to give dissociation rates significantly in excess of 10^3 s^{-1} to avoid a significant number of ions being collisionally cooled after activation.

The random walk simulation can be adapted to predict quantitatively the fraction of $(AG)_n$ ions expected to fragment following the input of 4 eV into a 300 K ion in the presence of the bath gas. Multiple random walk cooling simulations for $(AG)_n$ (n = 8, 12, 16) ions at initial energy $E_{300\,K+4\,eV}$ were performed and the results averaged to give composite $(AG)_n$ cooling curves similar to those shown in Fig. 3. Examining the internal energy evolution for each individual simulation, a dissociation was assumed to occur after ion-neutral collision n_{col} if the inequality in Eq. 25 was satisfied,

$$r_4 < \frac{k_{uni}(E_{n_{col}})}{k_{uni}(E_{n_{col}}) + \nu} \quad (25)$$

where r_4 is another random number. The dissociation results were histogrammed to give the fraction of $(AG)_n$ ions remaining as a function of cooling time, $t = n_{col}/\nu$. Fig. 4 shows the composite cooling and fragmentation curves for $(AG)_8$; the plots indicate that nearly all fragmentation [i.e. ~45% of the initial $(AG)_8$ population] should occur within ~500 μs,

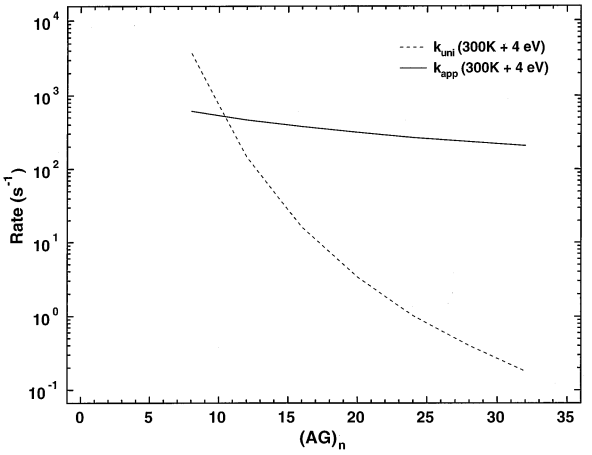

Fig. 3. Comparison of the unimolecular dissociation rate constant k_{uni} and the cooling rate k_{app} for $(AG)_n$-mers having internal energy equal to the average internal energy at 300 K plus that of a 308 nm (4 eV) photon.

during which time the $(AG)_8$ internal energy should fall to ~75% of its initial value. The internal energies E_t and corresponding $k_{uni}(E_t)$ values are indicated on the cooling curve ($k_{app} = 6.1 \times 10^2$ s^{-1}) for times t = 0, 100, and 500 μs. Because $k_{uni}(E)$ values over the initial 100 μs are considerably greater than k_{app}, approximately two thirds of the overall fragmentation occurs at an observed dissociation rate $k_{diss} = 2.9 \times 10^3$ s^{-1} that is between k_{uni} at t = 0 μs (3.7×10^3 s^{-1}) and t = 100 μs (1.8×10^3 s^{-1}). The remaining one third of the fragmentation occurs over a longer period (~400 μs) as $k_{uni}(E)$ gradually becomes less than k_{app} and thus, k_{diss} falls to essentially zero. By contrast, in the absence of cooling (i.e., k_{app} = 0), roughly 16% of the $(AG)_8$ ions would survive to 500 μs and about 2.5% would remain at 1 ms. Data from the other simulations indicated that >95% and 99% of the $(AG)_{12}$ ($k_{app} = 470$ s^{-1}) and $(AG)_{16}$ ($k_{app} = 380$ s^{-1}) ions, respectively, remained intact because their $k_{uni}(E)$ values were always much less than k_{app}. The results of this modelling study are in qualitative accord with ion-ion electron transfer results. For example, multiply charged oligonucleotide anions that undergo electron transfer with xenon cations are completely dissociated when there are four residues (~1.2 kDa) [29] but show no fragmentation when there are 12 residues (~3.6 kDa) [31].

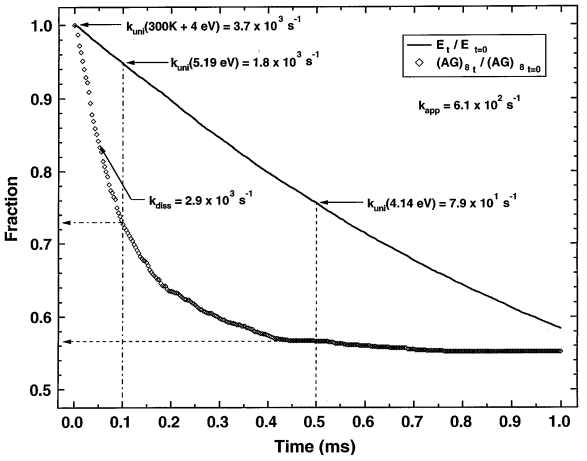

Fig. 4. Composite cooling curve and corresponding fraction of intact $(AG)_8$ ions following input of a 308 nm photon. The phenomenologic cooling rate $k_{app} = 6.3 \times 10^2\ s^{-1}$ and the observed dissociation rate $k_{diss} = 2.9 \times 10^3\ s^{-1}$. Unimolecular dissociation rate constants $k_{uni}(E)$ are also indicated for the initial internal energy (300 K + 4 eV) and for energies at cooling times of 100 (5.19 eV) and 500 (4.14 eV) μs.

4. Conclusions

The bath gas present in a typical Paul trap experiment plays an important role in determining the extent of fragmentation observed from high-mass (>1 kDa) ions after a rapid transitory input of internal energy, provided the ions behave statistically. Apparent collisional cooling rates determined via random walk simulation range from 10^2–$10^3\ s^{-1}$ when relatively small average energy down-step sizes are employed; cooling rates are somewhat higher using a diffuse scattering model. Collisional cooling rates tend to decrease slowly with ion size, whereas unimolecular dissociation rates at fixed internal energy decrease far more rapidly as ion size increases. Thus, if a rapid transitory input of energy is to be effective for activation of such ions, it must drive reactions in excess of $10^3\ s^{-1}$ in order to avoid collisional cooling of a large fraction of the activated ions.

Acknowledgements

Research sponsored by the Division of Chemical Sciences, Office of Basic Energy Sciences, U.S. Department of Energy, under Contract DE-AC05-96OR22464 with Oak Ridge National Laboratory, managed by Lockheed Martin Energy Research Corporation.

References

[1] M. Yamashita, J.B. Fenn, J. Phys. Chem. 88 (1984) 4451.
[2] M.L. Aleksandrov, L.N. Gall, N.V. Krasnov, V.I. Nikolaev, V.A. Paulenko, V.A. Shkurov, Dokl. Phys. Chem. (Eng.) 277 (1984) 572.
[3] J.B. Fenn, M. Mann, C.K. Meng, S.F. Wong, C.M. Whitehouse, Science 246 (1990) 64.
[4] R.D. Smith, J.A. Loo, C.G. Edmonds, C.J. Barinaga, H.R. Udseth, Anal. Chem. 62 (1990) 882.
[5] J.B. Fenn, M. Mann, C.K. Meng, S.F. Wong, C.M. Whitehouse, Mass Spectrom. Rev. 9 (1990) 37.
[6] R.D. Smith, J.A. Loo, R.R. Ogorzalek Loo, M. Busman, H.R. Udseth, Mass Spectrom. Rev. 10 (1991) 359.
[7] R.B. Cole (Ed.), Electrospray Ionization Mass Spectrometry, Wiley, New York, 1997.
[8] M. Karas, F. Hillenkamp, Anal. Chem. 60 (1988) 2299.
[9] A. Overberg, M. Karas, F. Hillenkamp, Rapid Commun. Mass Spectrom. 5 (1991) 128.
[10] E. Nordhoff, A. Ingedoh, R. Cramer, A. Overberg, B. Stahl, M. Karas, F. Hillenkamp, P.F. Crain, Rapid Commun. Mass Spectrom. 6 (1992) 771.
[11] C. Weickhardt, F. Moritz, J. Grotemeyer, Mass Spectrom. Rev. 15 (1996) 139.
[12] M. Guilhaus, V. Mlynski, D. Selby, Rapid Commun. Mass Spectrom. 11 (1997) 951.
[13] T. Dienes, S.J. Pastor, S. Schürch, J.R. Scott, J. Yao, S. Cui, C.L. Wilkins, Mass Spectrom. Rev. 15 (1996) 163.
[14] R.E. March, J.F.J. Todd (Eds.), Practical Aspects of Ion Trap Mass Spectrometry, Vols. I–III, CRC, Boca Raton, FL, 1995.
[15] S.A. McLuckey, Adv. Mass Spectrom., in press.
[16] G.C. Stafford Jr., P.E. Kelley, J.E.P. Syka, W.E. Reynolds, J.F.J. Todd, Int. J. Mass Spectrom. Ion Processes 60 (1984) 85.
[17] R.K. Julian Jr., R.G. Cooks, R.E. March, F.A. Londry, in R.E. March, J.F.J. Todd (Eds.), Practical Aspects of Ion Trap Mass Spectrometry, Vol. I, CRC, Boca Raton, FL, 1995, Chap. 6.
[18] J.N. Louris, J.W. Amy, T.Y. Ridley, R.G. Cooks, Int. J. Mass Spectrom. Ion Processes 88 (1989) 97.
[19] S.A. McLuckey, G.L. Glish, K.G. Asano, Anal. Chim. Acta 225 (1989) 25.
[20] S.A. McLuckey, G.J. Van Berkel, G.L. Glish, J.C. Schwartz, in R.E. March, J.F.J. Todd (Eds.), Practical Aspects of Ion Trap Mass Spectrometry, Vol. II, Ion Trap Instrumentation, CRC, Boca Raton, FL, 1995, Chap. 3, pp. 89–141.
[21] S.A. McLuckey, G.J. Van Berkel, D.E. Goeringer, G.L. Glish, Anal. Chem. 66 (1994) 689A–696A.
[22] J.C. Schwartz, R.E. Kaiser Jr., R.G. Cooks, P.J. Savickas, Int. J. Mass Spectrom. Ion Processes 98 (1990) 209.
[23] D.E. Goeringer, S.A. McLuckey, J. Chem. Phys. 104 (1996) 2214–2221.

[24] D.E. Goeringer, S.A. McLuckey, Rapid Commun. Mass Spectrom. 10 (1996) 328–334.
[25] S.A. McLuckey, R.S. Ramsey, J. Am. Soc. Mass Spectrom. 5 (1994) 324–327.
[26] M.J. Doktycz, S. Habibi-Goudarzi, S.A. McLuckey, Anal. Chem. 66 (1994) 3416–3422.
[27] J.L. Stephenson Jr., S.A. McLuckey, J. Am. Chem. Soc. 118 (1996) 7390–7397.
[28] J.L. Stephenson Jr., G.J. Van Berkel, S.A. McLuckey, J. Am. Soc. Mass Spectrom. 8 (1997) 637–644.
[29] W.J. Herron, D.E. Goeringer, S.A. McLuckey, J. Am. Chem. Soc. 117 (1995) 11555–11562.
[30] S.A. McLuckey, J.L. Stephenson Jr., R.A.J. O'Hair, J. Am. Soc. Mass Spectrom. 8 (1997) 148–154.
[31] J.L. Stephenson Jr., S.A. McLuckey, Rapid Commun. Mass Spectrom. 11 (1997) 875–880.
[32] G.W. Flynn, C.S. Parmenter, A.M. Wodtke, J. Phys. Chem. 100 (1996) 12817.
[33] K.A. Boering, J.I. Brauman, J. Chem. Phys. 97 (1992) 5439.
[34] T. Wyttenbach, M.T. Bowers, J. Phys. Chem. 97 (1993) 9573.
[35] S. Kato, V.M. Bierbaum, S.R. Leone, Int. J. Mass Spectrom. Ion Processes 149/150 (1995) 469.
[36] E.M. Marzluff, S. Campbell, M.T. Rodgers, J.L. Beauchamp, J. Am. Chem. Soc. 116 (1994) 6947.
[37] E.W. Schlag, R.D. Levine, Chem. Phys. Lett. 163 (1989) 523.
[38] L.L. Griffin, D.J. McAdoo, J. Am. Soc. Mass Spectrom. 4 (1993) 11.
[39] S.A. McLuckey, W.J. Herron, J.L. Stephenson Jr., D.E. Goeringer, J. Mass Spectrom. 31 (1996) 1093–1100.
[40] W. Forst, Theory of Unimolecular Reactions, Academic, New York, 1973.
[41] R.C. Dunbar, J. Chem. Phys. 90 (1989) 7369.
[42] R.C. Dunbar, J. Phys. Chem. 98 (1994) 8705.
[43] D.T. Gillespie, J. Phys. Chem. 81 (1977) 2340.
[44] D.C. Tardy, B.S. Rabinovitch, Chem. Rev. 11 (1977) 369.
[45] T.T. Nguyen, K.D. King, R.G. Gilbert, J. Phys. Chem. 87 (1983) 494.
[46] K.D. King, T.T. Nguyen, R.G. Gilbert, Chem. Phys. 61 (1981) 223.
[47] R.G. Gilbert, J. Chem. Phys. 80 (1984) 5501.
[48] R.G. Gilbert, K.D. King, Chem. Phys. 19 (1980) 367.
[49] R.V. Serauskas, E.W. Schlag, J. Chem. Phys. 45 (1966) 3706.
[50] R.C. Bhattacharjee, W. Forst, Chem. Phys. 30 (1978) 217.
[51] W. Forst, R.C. Bhattacharjee, Chem. Phys. 37 (1979) 343.
[52] A.T. Barfknecht, J.I. Brauman, J. Chem. Phys. 84 (1986) 3870.
[53] H.E. Revercomb, E.A. Mason, Anal. Chem. 47 (1975) 970.
[54] Y.-L. Chen, B.A. Collings, D.J. Douglas, J. Am. Soc. Mass Spectrom. 8 (1997) 681.
[55] W. Forst, Z. Prásil, J. Chem. Phys. 51 (1969) 3006.
[56] M.R. Hoare, T.W. Ruijgrok, J. Chem. Phys. 52 (1970) 113.
[57] J.R. Barker, Chem. Phys. 77 (1983) 301.